

Towards an understanding of the self-healing capacity of asphaltic mixtures

N. Kringos, A. Schmets, A. Scarpas

Delft University of Technology, Delft, the Netherlands

T. Pauli

Western Research Institute, Wyoming, USA

The self-restoring or healing capacity of asphalt has been known for quite some time. Yet, to this date, there is no consensus of the fundamental mechanism underlying this phenomenon. In this paper a multi-scale model is presented which focuses on the healing phenomenon from a thermodynamic point of view. In the model, healing of bituminous material is simulated at the micro scale via a phase field model, utilizing a modified version of the Cahn Hilliard and Flory-Huggins equations. This model is then connected to a more general elasto-visco-plastic constitutive framework for the simulation of asphalt mixtures. The paper presents the developed hypothesis, the experimental evidence and summarizes some of the theoretical background. The model has been implemented in the 3D finite element system CAPA-3D and preliminary results are shown.

1 Introduction

1.1 *Self healing ability of bitumen*

Over the last two decades various laboratory experiments have shown clear evidence of the beneficial effects of rest periods in restoring the stiffness and strength characteristics of asphaltic samples subjected to fatigue loading [e.g. Jones and Kennedy 1991, Philips 1999, Hammoumm et al. 2002, Lu X. et al. 2003, Little and Bhasin 2007]. There is consensus among researchers that cracking failure prediction models grossly underestimate asphalt concrete pavements field life and it is accepted that the reason for this discrepancy is largely the exclusion of healing effects from design calculations.

Over the years, researchers have tried to understand the healing in bituminous materials from a purely mechanical point of view. Unfortunately, this approach has not resulted into a consistent picture for the healing behaviour nor has it had the impact on production and

design which it could have, once properly understood. So far, the fundamental mechanisms of the chemical and physical interactions within asphaltic concrete responsible for healing at crack faces are merely speculations rather than based on thorough scientific analysis. Moreover, some of the speculated healing mechanisms all exploit the comparison with high molecular weight polymer systems [Kim Y.R. et al 1990, Little and Bhasin 2007], whereas bitumen has a more complex composition, and consists of thousands of very different organic molecules, allowing for a very rich variety of interactions.

Considering the importance and uniqueness of the healing phenomenon in bitumen, an international research consortium was set-up to investigate the fundamental mechanisms and develop a model which enables the accurate prediction. In this paper an overview of the developed model within the framework of this research project and its theoretical and experimental background is given.

1.2 Wax induced phase-separation

Using Atomic Force Microscopy (AFM) scans, various types of bitumen were studied. Intermittent-contact Wave-Mode AFM was used to collect both topography and phase-contrast images of bitumen prepared in thin films on glass microscope slides. During the Strategic Highway Research Program (SHRP) in the late 80ties and early 90ties, in the USA, several bitumen were investigated and extensively characterized. These bitumen are referred to as “SHRP core bitumen”. For the AFM investigation in this research, various SHRP core bitumen were selected based on differences in thermal characteristics as measured by the activation energy of viscous flow [3]. Samples of bitumen and their fractions were prepared for investigation under the AFM. In some experiments the temperature of the sample could be increased in an incremental fashion, then held at a constant temperature prior to collecting an AFM image, then incrementally decreased and again held constant at various temperatures prior to imaging the specimen. Height (topography) and phase images were recorded and compared based on bitumen crude source.

Figure 1 and Figure 2 only depict AFM Wave-Mode topography images of neat SHRP bitumen. In these figures, the bitumen are better ranked in terms of crystalline wax content, χ_{crys} , based on DSC data [28], see Table 1, rather than asphaltene content as suggested in studies reported by other investigators [e.g. 15]. The one bitumen which does

not fit this observationally based trend is asphalt AAM-1. Number average molecular weights listed in Table 1, measured by VPO, which average around 801 ± 71 Daltons for the remaining seven asphalts may suggest that this asphalt is compositionally different and could be considered an outlier for this analysis. The micro-structural features that are depicted in these images have been serendipitously nick-named bumble-bees [15] apparently due to their resemblance to the black and yellow stripes and pointed end shape reminiscent of that of the topside a bumble-bee. To further investigate these structures, maltene materials derived from dissolution/filtration techniques and neutral fraction material generated by an ion exchange chromatography technique for separating polar and

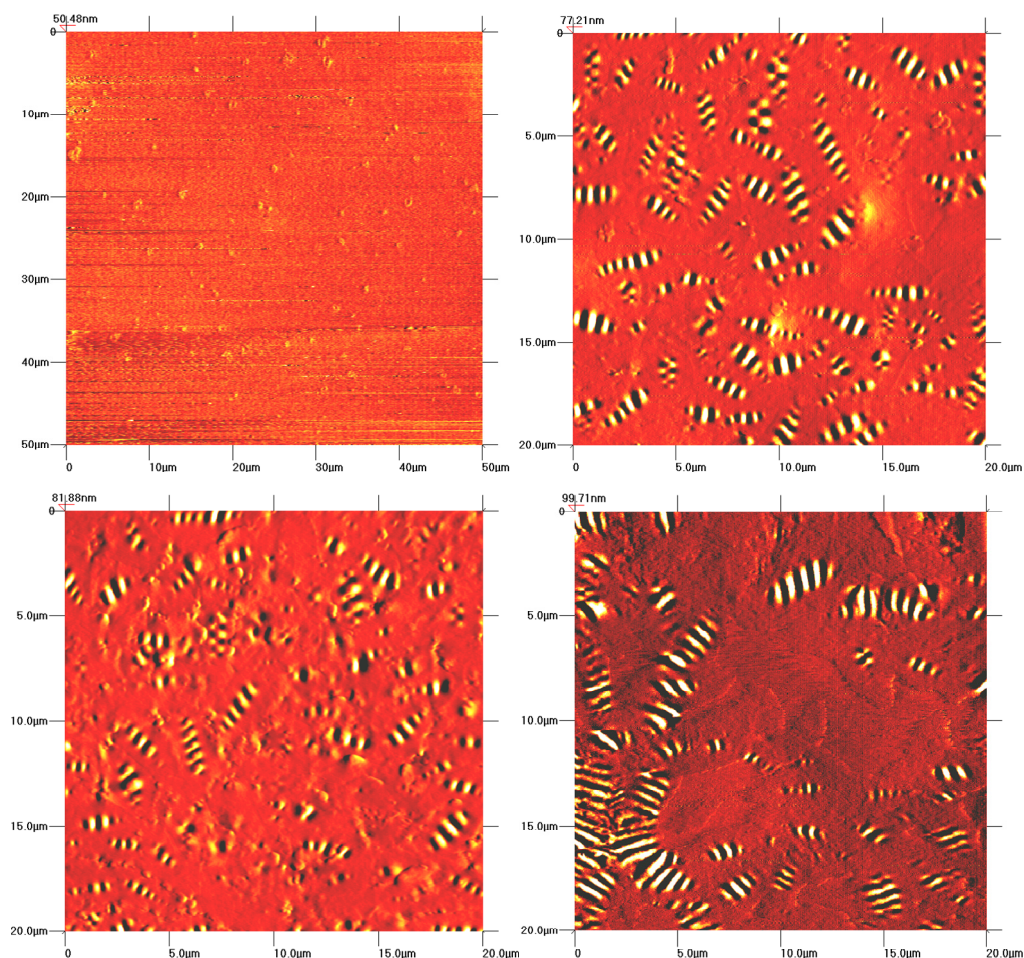


Figure 1: AFM Wave-Mode topography images of neat SHRP bitumen (from left to right and top to bottom); AAA-1, AAB-1, AAC-1 and AAD-1 [25]

non-polar material fractions were derived from these eight bitumen and studied by intermittent-contact AFM. Figure 3 depicts the scans of bitumen AAK-1 and AAC-1, and maltenes and IEC neutral fractions of these two asphalts. The “bumble-bee” structures are readily observed in all of the images depicted. Investigation of the neutral fractions for the other six bitumen revealed that bumble-bee structures were also observed [25].

Similar images of bitumen samples have been recorded by another, high resolution (VEECO) AFM setup. Bitumen samples were prepared by dropping the molten material (180 °C) on aluminium sample holders for the AFM. The AFM was equipped with a

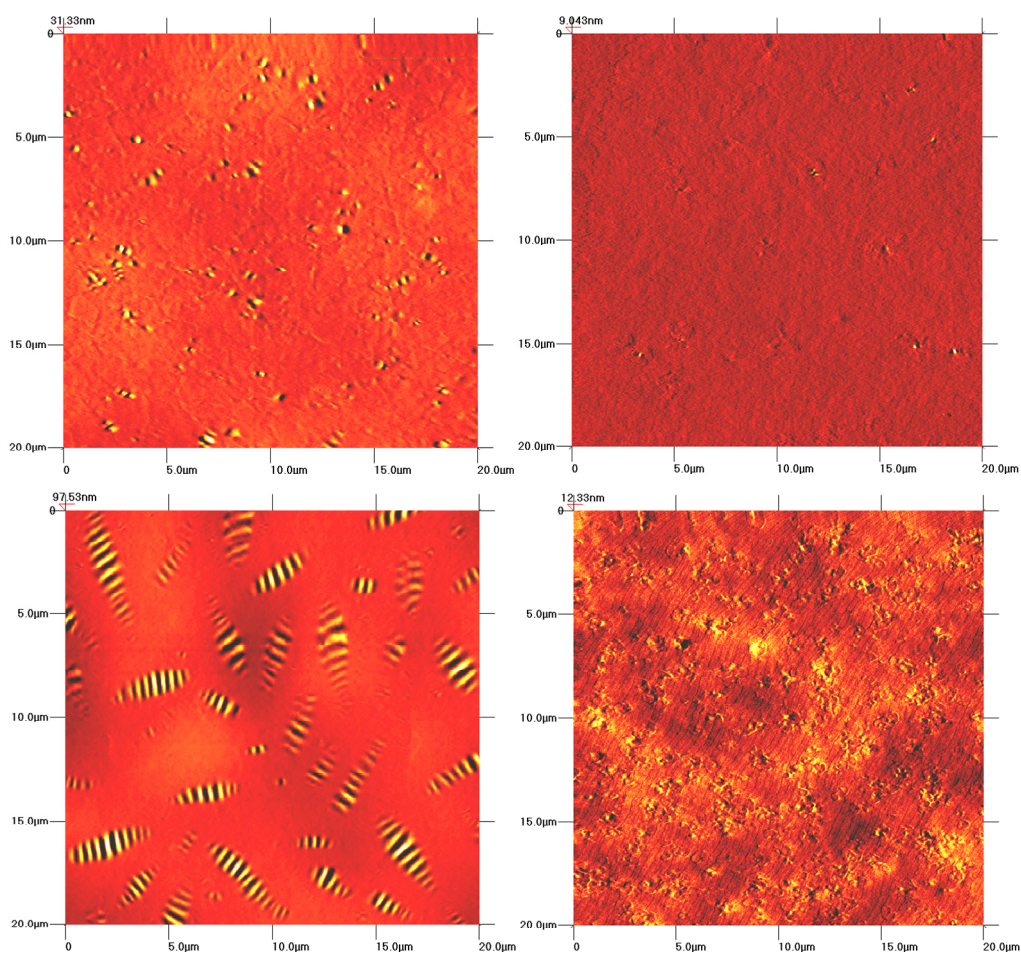


Figure 2: AFM Wave-Mode topography images of neat SHRP asphalts (from left to right and top to bottom); AAF-1, AAG-1, AAK-1 and AAM-1 [25]

Table 1: Compositional properties measured for the eight SHRP “core” bitumen

Sample	^a Number average Molecular weight, M_n , Daltons	Percent asphaltenes n-heptane insoluble	^b χ_{cryst}
AAA-1	790	15.8	0.001
AAB-1	840	17.3	0.025
AAC-1	870	9.9	0.029
AAD-1	700	20.2	0.010
AAF-1	840	13.4	0.024
AAG-1	710	5.0	0.002
AAK-1	860	20.1	0.013
AAM-1	1300	3.7	0.037

^a Number average molecular weight by vapour phase osmometry in toluene at 60°C [3]

^b Crystalline fraction content determined by differential scanning calorimetry (DSC) referenced in [Turner and Branthaver, 1997]

heating stage and a (Peltier) cooling stage, giving access to sample temperatures between -40 °C and 200 °C. The temperature dependent results of this experimental campaign will be published in a separate paper. Some typical examples of these AFM images from a bitumen that was close to the SHRP AAC-1 at room temperature are shown in Figure 4. These high resolution images reveal considerable extra detail compared to those presented in Figures 1 through 3. Especially at the higher magnification (right figure) new, previously not observed details become visible: pronounced crystalline micro-structuring, i.e., ledge and terrace assemblages. This structuring is not unlike findings for similar studies involving model waxes [7, 30, 4, 8]. All this strongly suggests that the observed bee structures consist mainly out of waxes.

1.3 Phase separation throughout the bulk

Even though the above sections give a clear indication of wax-induced phase separation in bitumen, the evidence has been mainly focused on two dimensional films of bitumen. This would leave the possibility that the separating out of the waxes is an effect that occurs at the surface instead of the bulk, due to a surface tension effect. Since the existence of a phase separation phenomenon in bitumen is at the basis of the developed healing model, presented later on in this paper, it is important to ensure that phase separation is in fact a bulk property.

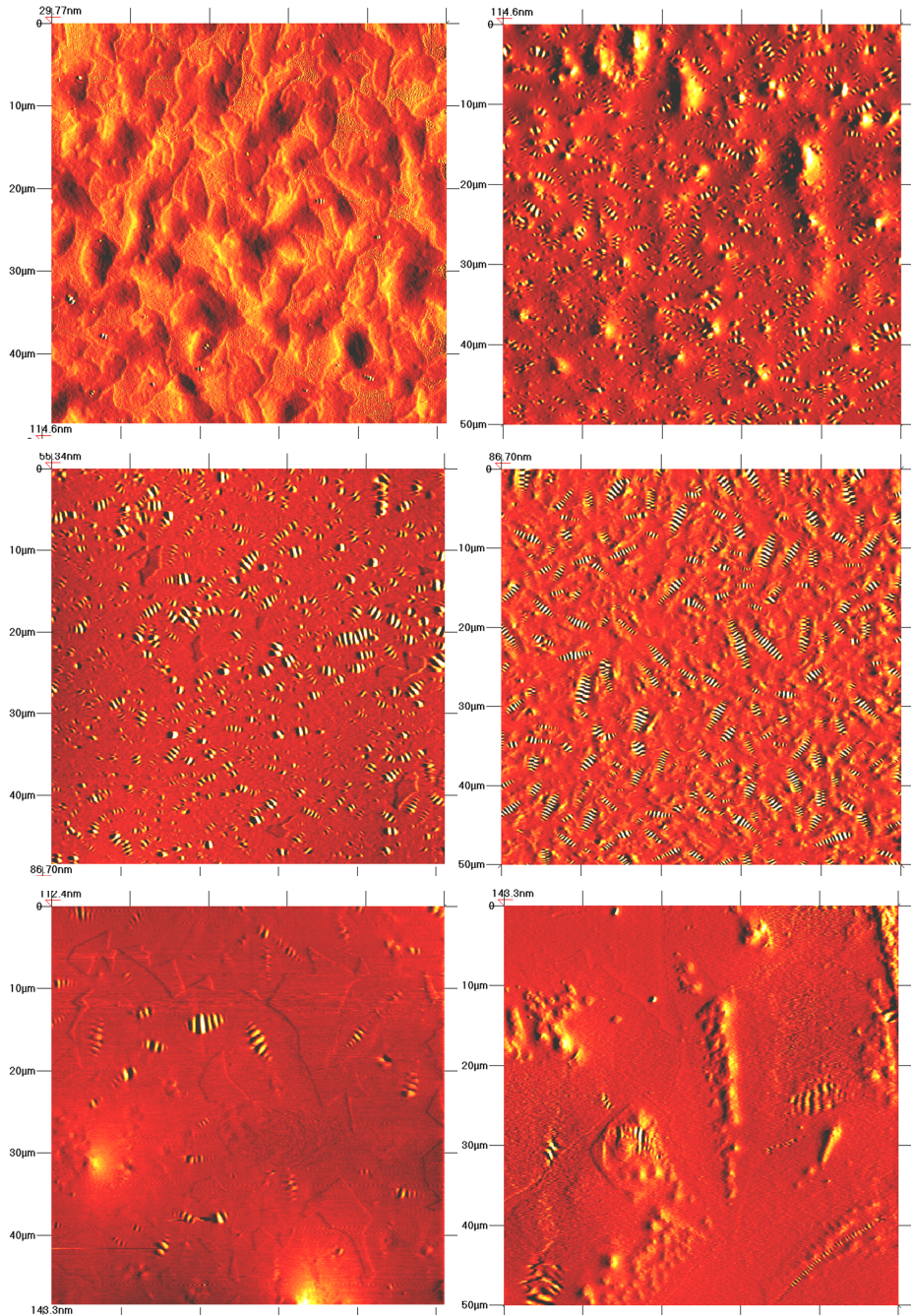


Figure 3: AFM Wave-Mode topography images of two neat SHRP asphalts AAK-1 (left image set) and AAC-1 (right image set), (top), and asphalt fractions; maltenes (middle) and IEC-neutrals (bottom) [25].

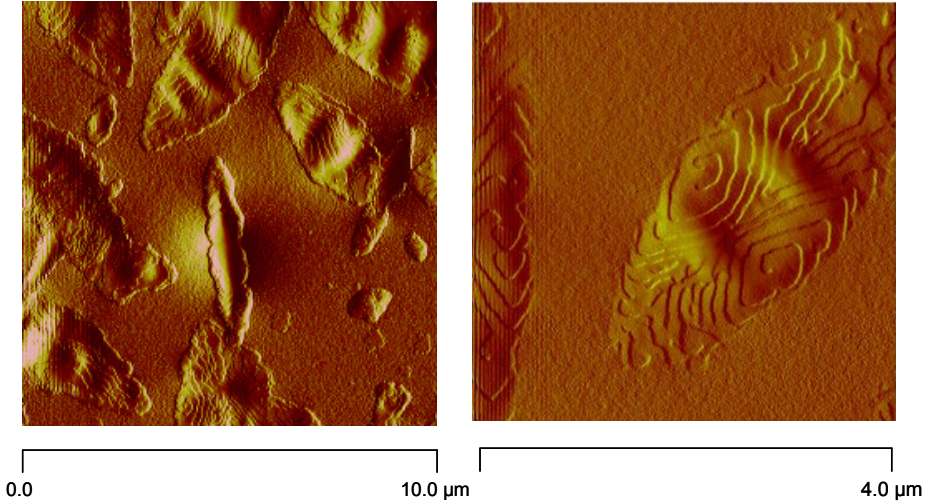


Figure 4: Terracing structure of AFM phases observed in tapping mode with a VEECO AFM (located at TU Delft). The bitumen imaged was in composition close to the SHRP AAC-1 bitumen.

To address this issue, Small Angle Neutron Scattering (SANS) experiments have been performed on the Spin Echo Small Angle Neutron Scattering (SESANS) spectrometer at the Reactor Institute Delft, Figure 5 [24]. Complementary quasi-elastic neutron scattering experiments have been conducted with the NEAT spectrometer at the Hahn-Meitner Institut, Berlin [14]. The first facility, SESANS, allows for the ‘in bulk’ determination of density-density correlation function, i.e. it correlates the (scattering length) density $\rho(\vec{r})$ at any location \vec{r} in the sample with the density $\rho(\vec{r}')$ at any other location \vec{r}' in the sample. Such a density-density correlation function is usually written as

$$\gamma(r) = \langle \rho(0)\rho(r) \rangle. \quad (1)$$

In a SANS experiment the Fourier transform of this correlation function is measured. This implies that by an inverse Fourier transformation the real-space density-density correlation function as well as the closely related pair correlation function can be retrieved [10]. In case of a sample with a two-phase morphology, the two distinct substances can in principle be distinguished easily by small angle scattering techniques. The only requirements are that i) the length scale of an average phase-domain is within the observable range of the small angle technique (between several nanometres up to micrometers when the SESANS technique is utilized [24]) and ii) the distinct phases in the sample should be ‘sufficiently

different' for neutrons. The latter requirement means that the phases should have a distinct scattering length density [16]. Given the enormous scattering cross section of hydrogen atoms, local variations in the hydrogen-to-carbon ratio (H/C-ratio) of 5% will provide enough scattering contrast to distinguish the phases. This all implies that whenever a small angle signal is observed that there is a kind of ordering or domain structure present in the sample. In principle, however tedious it may be, one can back calculate from the observed scattering data to the scattering length density, hence the average molecular make-up of the phases.

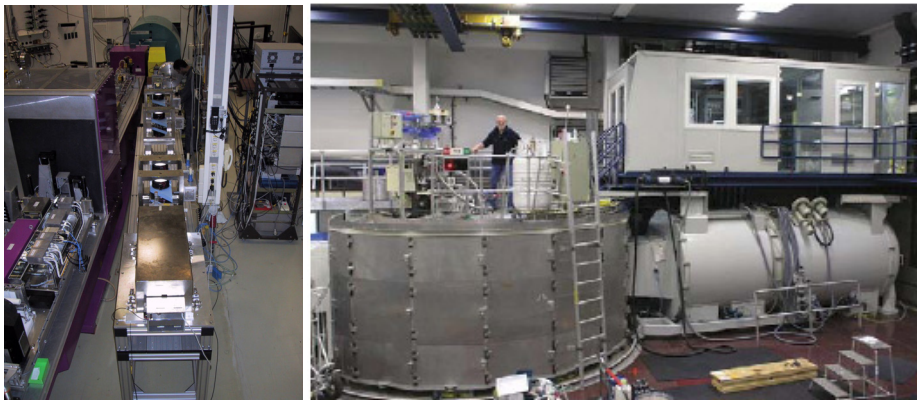


Figure 5: Spin Echo Small Angle Neutron Scattering, SESANS, set-up at Reactor Institute Delft, TU Delft (left) and the inelastic neutron scattering spectrometer NEAT at the Hahn Meitner Institut, Berlin (right).

Comparing the observed SANS response with surface and bulk models enables to decide whether the structural features that were observed at the bitumen's surface, are also present in the bulk of the material. It should be noted that traditional small angle techniques could never observe this effect, since they are limited to lengths up to several tens of nanometres, while the observed features have length in the range of micrometers, which is accessible by the SESANS setup [24].

The microscopic structure and dynamics of the selected bitumen grades have been studied by quasi-elastic neutron scattering. With this technique one obtains the Fourier transform of the 4-dimensional space-time or van Hove correlation function [16, 2]. All structural and dynamical information of the system under scrutiny can be extracted from this.

To investigate the mobility of the bitumen phases, neutron scattering experiments were carried out at the NEAT spectrometer at the Hahn-Meitner Institut. The experiments were conducted for various bituminous samples and at various temperatures, so that the temperature dependence of the dynamical phenomena could be obtained. An illustrative example of the observed dynamical structure factor at a wave-vector $Q = 0.8 \text{ \AA}^{-1}$ for the various temperatures is displayed in Figure 6. From this experiments it was found that, within the experimental window, the observed peak shape is best described by the convolution of two Lorentzians (in energy); i.e. within the experimental window the observed pattern can be described by a 2-component model, each component having a distinct diffusion constant D . In this, the D is proportional to the Lorentzian line width. Moreover, there are two meaningful qualitative features visible in the observed pattern in Figure 6. Firstly the presence of the elastic peak (at zero meV energy transfer) indicates firmly that the diffusing particles are 'space-bound', i.e. they are not diffusing through all the material, but can access only a limited area [2]. Secondly, while going up in temperature an asymmetry sets in at the neutron energy loss site of the spectrum. This asymmetry can not be explained by a detailed balance effect [16], and can be identified with a Boson peak [27], a signature that the system's dynamics resembles that of a typical glass.

Furthermore, from the first results of the SANS experiments, it was observed that the bitumen exhibits a two-phase morphology, and that the two phases are chemically distinct in nature (suggested by the variation of H/C ratio over the regions), Figure 7. For bitumen

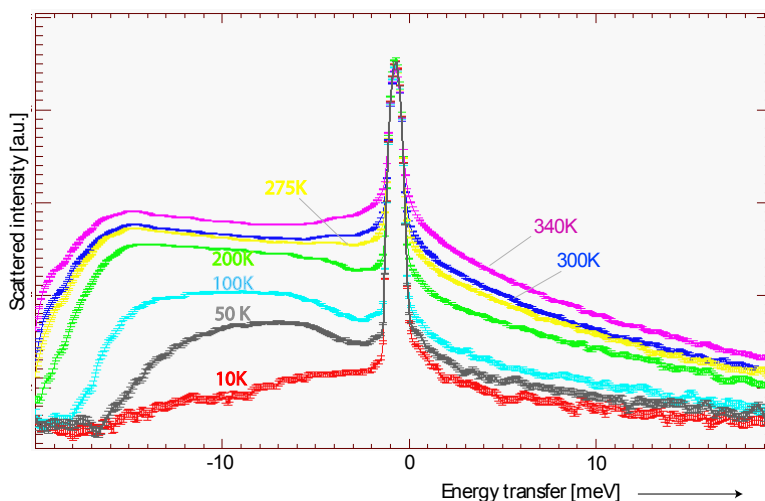


Figure 6: Temperature dependence of the scattering function for a single angle. Here $Q = 0.8 \text{ \AA}^{-1}$.

with bee-structures the SANS-signal starts decreasing from 10 μm on, a length comparable to the size of the bee-structures, whereas the signal stays constant for bitumen without bee-structures.

With rapid quenching of liquid bitumen to low temperatures, the two-phase morphology was not visible, but with slow cooling a two phase system was again apparent. The simplest plausible model to explain the facts observed is to assume that the material consists out of two types of moieties (or one type of moiety, and an amorphous remainder). Also, the ordering process appears to be slow and temperature dependent, hence it may be diffusive in nature.

Yet bitumen possesses a continuous range of properties, due to their very complicated composition [22]. This means that the exact potential energy landscape of the system can never be obtained. The only way to deal with this inherent complexity is to adopt mean field theories, where exact interactions are averaged and smeared out. The issue is then whether a two component system, as presented in this paper, is not in contradiction with the very (complicated) nature of bitumen. This appears not to be the case, as long as the formation of a phase does not require three-particle correlations. The proof is as follows:

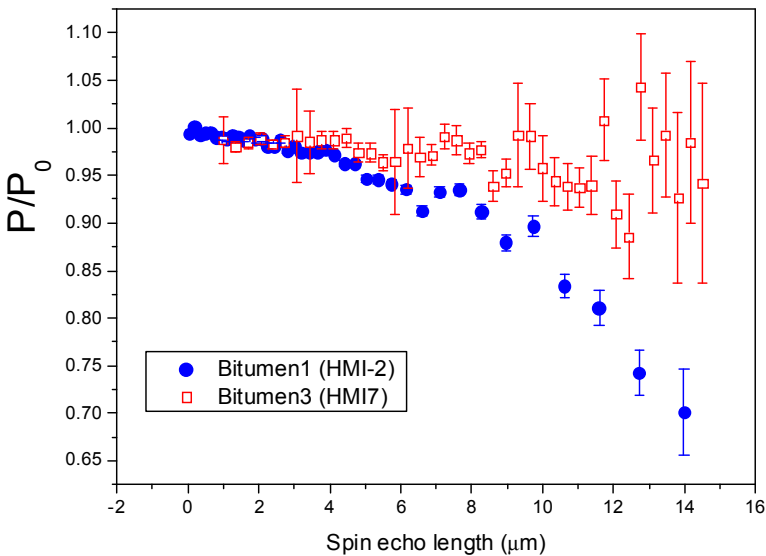


Figure 7: SANS signal of bitumen without bee-structures (red open squares) and with bee structures (blue, solid circles), in which P/P_0 is the depolarization.

Select a molecular species present in the system. We wish to compare a property of this molecule with the same property of any other molecule present in the system. The properties are either 'compatible' or 'not compatible', which leads to a natural separation in two phases. This reasoning appears somewhat radical, because we do not allow properties to be 'more or less compatible'. However this is merely a matter of energy barriers (thermal activation required) than of chemical compatibility. Demonstrations of a system with continuously distributed properties *and* two phase morphology, have been given in literature [1, 29]: polydisperse hard plate systems, and also in polydisperse hard sphere systems, show the formation of liquid crystalline phases. The driving forces for this separation are size exclusion or depletion effects.

It can therefore be concluded from the AFM experiments as well as from the neutron scattering experiments that bitumen can appear as if it were a binary system, although the properties of the constituent particles may vary in continuous manner. It is an important task to understand when and why this simple picture of bitumen as a binary liquid holds, and how this relates to the macroscopic behaviour of the material in real-world applications.

1.4 *Healing mechanism postulate*

From the extensive Atomic Force Microscopy and SANS experiment shown in the previous sections, it has become clear that bitumen has the tendency to phase separate under certain kinetic conditions. From the AFM scans it can be seen that this separation leads to a predominant clustering of two types of phases, α and β , illustrated in Figure 8. From mechanical considerations, it is known that the interfaces between two materials

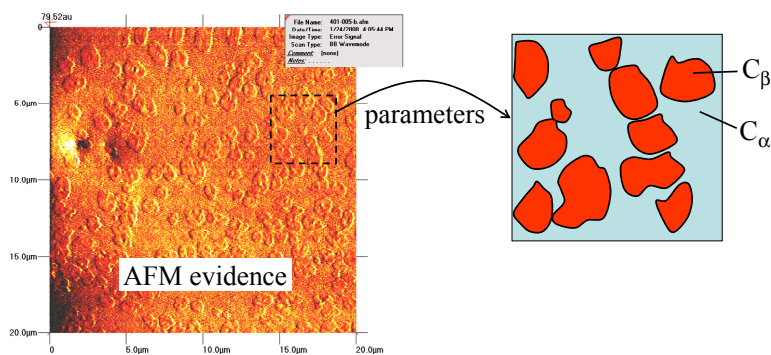


Figure 8: AFM evidence of phase-separation in bitumen [Pauli 2001]

with different stiffness properties serve as natural stress inducers. This means that when the material is exposed to mechanical and or environmental loading, these interfaces will attract high stresses and are prone to cracking. On this scale, this would result into a crazing pattern which can be detected on a macro-scale by a degradation of the mechanical properties of the material. If this process would continue, these micro-cracks (crazes) would continue developing, start merging and finally form macro-cracks. As a demonstration of the concept of diminished response and the introduction of high stresses in an inhomogeneous material, a finite element simulation is shown in Figure 9 in which a constant displacement is imposed on a homogeneous and an inhomogeneous bitumen. The bituminous matrix is hereby simulated as a visco-elastic material and the inclusions as elastic. From the deformation pattern it can be clearly seen that the inhomogeneous material acts not only stiffer, but is also no longer deforming in a smooth, uniform, manner.

From the AFM and neutron scattering experiments it was shown that bitumen, under certain circumstances, can form such inhomogeneities. If then, by changing the thermodynamic conditions of the material, for instance by inputting thermal or mechanical energy, these inclusions would disappear; restoration of the mechanical properties would appear on a macro-scale. Since the phase-separation is occurring on the nano-micro scale,

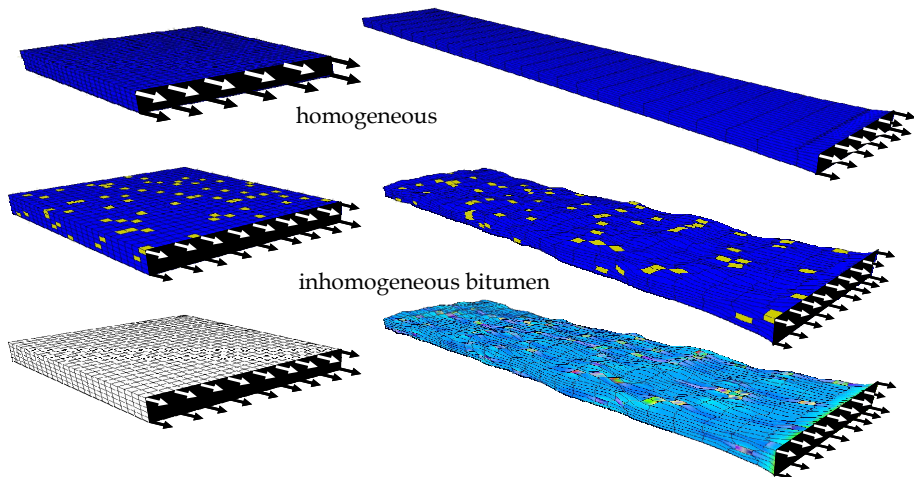


Figure 9: Displacement and normal stress development in a homogeneous vs inhomogeneous bitumen

the interfaces between the clusters and the matrix could start crazing when exposed to mechanical loading. A change of these clusters, either by rearranging themselves or by merging into the main matrix, would then lead to a memory loss of these crazes and the bitumen would show a restoration of its original properties, otherwise referred to as “healing”.

In this project, this re-arrangement of the phases is modelled with a so-called phase field theory and serves as a basis of the finite element based healing model for asphalts. The driving force for the rearrangement of the phases upon a changed thermodynamic state is explained in the following.

2 Kinetics of phase separation

The choice of the appropriate scale to describe a material depends on the type of information required about the system under consideration. Macroscopic quantities, which reflect the physico-chemical properties of the studied material are closely connected with the characteristics of single particles (i.e. atoms, molecules or phases). So, for instance, the temperature is connected with the mean energy of the thermal motion of the particles, the mass density straightforwardly depends on the mean number of particles in unit volume, etc. Thus, the description of the system at the macroscopic level reflects its microscopic characteristics.

To study the properties of phase separating material, a certain number of its macroscopic characteristics, i.e. state variables, must be identified. The set of independent macroscopic parameters then represents the state of the system under consideration. The thermodynamic state of the system is given by the complex of all the external conditions acting on the system and also by the set of the independent properties of the system. If all macroscopic parts of the given system exist in the same state when the system as a whole is in the equilibrium state, the system is called homogeneous.

In the classical thermodynamic description of a system in chemical equilibrium the given phase areas in the phase diagrams represent zones of minima of the Gibbs energy, whereas the phase coexistence is given by the Gibbs phase rule. To construct such a phase diagram requires the mapping of all available phases and locating their phase boundaries which,

unfortunately, is not possible by mere direct measurements of temperature or concentration dependences of the change of the Gibbs potential.

Equilibrium phase diagrams, however, cannot say anything about the reaction which transforms one phase to another, nor about the composition or the structure of phases occurring under conditions different from those that make equilibrium possible.

Under conditions of phase equilibrium, when the chemical potential of the phase α , $\alpha\mu$ is equal to that of phase β , $\beta\mu$, stable coexistence of both phases occurs. For a real material, however, the system temperature deviates from the equilibrium one for which the equality of chemical potentials is violated, producing thus a driving force of the phase separation. The measure of this force is the chemical potential difference

$$\Delta\mu = \alpha\mu - \beta\mu \tag{2}$$

In other words, for $\Delta\mu < 0$ the phase β fraction, βc , will diminish and the fraction of phase α , αc , will increase. For $\Delta\mu > 0$ the reverse will happen. The phase fractions can therefore only be changed under non-equilibrium conditions of a definite driving force.

There are cases where the slowness of phase transformation can considerably affect the equilibrium. For instance, in an under-cooled liquid the meta-stable phases can be frozen and if the viscosity rapidly increases with decreasing temperature the vitreous state can freeze-in, resulting in an unstable solid state called glass transition. The time dependence of phase transition is therefore important for a better understanding of the relevant transformation kinetics locating at the same time the actual phase boundary between the two phases investigated.

The main processes that take place during phase separation and which influence the results of the whole process are the conditions (e.g. pressure or temperature) under which the new phase arises in the system and the structure of its composition; the nucleation of the new phase, first they arise and then they grow (i.e. the kinetics of the phase transformation) and the transport of energy and mass in the system.

The total Gibbs energy of a biphasic system is

$$G = N \left[{}_1c {}_1\mu + (1 - {}_1c) {}_2\mu + k_B T \{ {}_1c \ln {}_1c + (1 - {}_1c) \ln (1 - {}_1c) + H({}_1c, {}_2c, T) \} \right] \quad (3)$$

with ${}_1c + {}_2c = 1.0$

where ${}_a c$ is the concentration of component α in the system, N is the total number of molecules, ${}_a \mu$ are the chemical potentials per atom of the component α , $k_B = R/N$ is the Boltzman constant, relating energy at the molecule level with temperature T observed at the bulk level, and H is the Gibbs mixing energy per molecule.

From Eq. (3), the Gibbs energy, otherwise known as the configurational free energy Ψ_0 , can also be written as

$$\Psi_0 = {}_1c {}_1g + (1 - {}_1c) {}_2g + RT \{ {}_1c \ln {}_1c + (1 - {}_1c) \ln (1 - {}_1c) + H \} \quad (4)$$

In equilibrium conditions it must hold that

$$\frac{\partial \Psi_0}{\partial c} = 0; \quad \frac{\partial \Psi_0}{\partial N} = 0 \quad (5)$$

An example of two equilibrium phase transformations is shown in Figure 10. It is possible that for kinetic reasons (e.g. very fast cooling, slow nucleation or growth etc.) the first phase transformation is not realized and the phase transitions that correspond to the lower temperature assert themselves. This would result in a change of the phase diagram and a new equilibrium or meta-stable state will form, Figure 11.

On the basis of the construction of the common tangent, the concentrations of the equilibrium or meta-stable phases which fulfill Eq. (5) can be found. Cahn and Hilliard [1958] formulated the continual theory of phase transition based on the change of the free energy during the phase transformation in the form:

$$\Delta F = \int_V \left[\Delta f' + k_{CH} (\nabla C)^2 \right] dV \quad (6)$$

where V is the volume of the new phase and

$$\Delta f' = f'(C) - f'(C_0) - (C - C_0) \left. \frac{\partial f'}{\partial C} \right|_{c=\bar{c}} \quad (7)$$

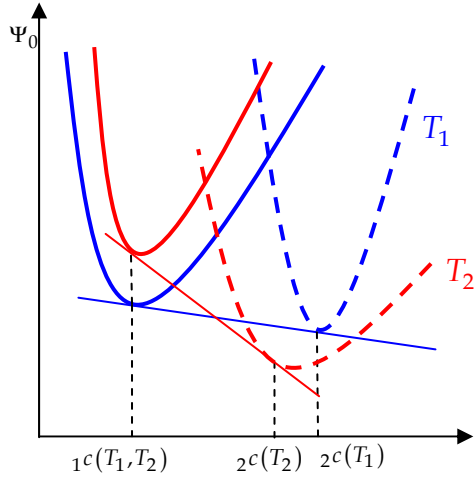


Figure 10: Equilibrium coexistence of two phases at temperature T_1 and T_2 , $T_1 > T_2$

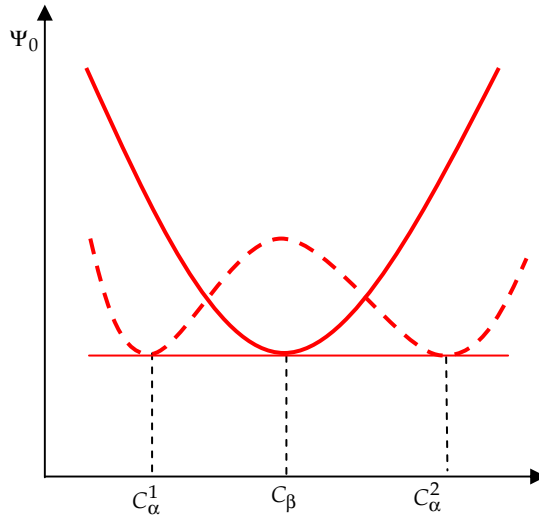


Figure 11: A possible dependence of Ψ_0 on the concentration C at equilibrium temperature T_E

where $f'(C)$ is the free energy per unit volume of the homogeneous system with the concentration C , \bar{C} is the mean value of the concentration in the system and k_{CH} is a constant.

The dynamics of the 1st order phase transformation under non-equilibrium conditions at a given constant temperature can proceed essentially via two mechanisms: in the nucleation and the following growth of overcritical nuclei or in the spinodal decomposition. The spinodal decomposition appears in systems that are rapidly cooled to unstable states delimited by a curve – the spinodal. The nucleation occurs in the meta-stable region between the binodal (corresponding to the equilibrium coexistence of phases) and the spinodal, Figure 12.

The spinodal corresponds to the inflection point on the curve $\Psi_0(\alpha c)$ at the temperature T . On the spinodal the following equation holds:

$$\frac{\partial \Psi_0}{\partial c^2} = 0 \tag{8}$$

For thermodynamic reasons a composition barrier exists in the meta-stable region, meaning that the system is unstable only regarding large changes of composition and it is stable regarding small fluctuations for which the free energy of the system increases. This barrier results in a relatively long-term stability of meta-stable states. Thus, in the meta-

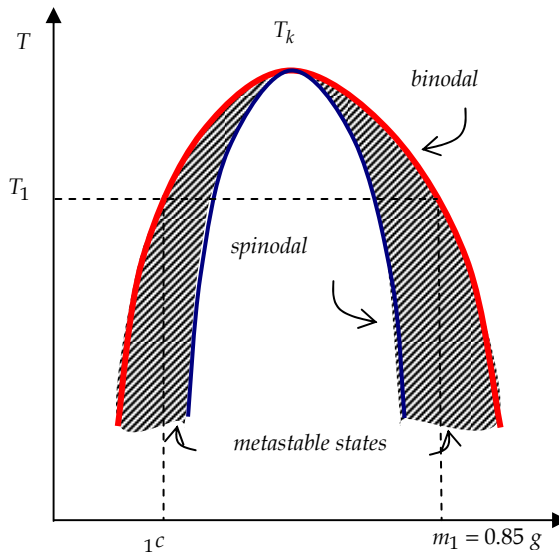


Figure 12: Coexistence of two phases at T_1

stable region the phase change proceeds by the nucleation mechanism, when only the overcritical nuclei grow with the critical composition.

Another situation is under the spinodal in the unstable region. In this region the composition barrier does not exist and the system is unstable even regarding small fluctuations of composition, which results in a decrease of the total energy of the system. The morphology is thus different in meta-stable and unstable regions.

Above the spinodal large changes of composition with a sharp phase interface are necessary for the phase transformation. Under the spinodal, however, every small change of the composition steadily increases to attain the difference of composition between the two phases given by the equilibrium phase diagram. At the beginning the differences between the phases are not sharp and a periodic shape of composition appears.

These mechanisms of phase transformation describe the evolution of the system at constant temperature and they do not answer the question, when and what metastable state is formed during rapid changes in temperature.

It is important to make sure that the observed material behaviour is not merely an artefact of the test method. For instance, liquid flow originating from the gradient of surface tension along the free surface due to temperature or concentration inhomogeneity (i.e. Marangoni flow) and/or to different curvature. This effect is weak under normal conditions and becomes more important in microgravity experiments with a free surface formed in space or in melt spinning techniques when thin films are formed. For this reason, in addition to AFM tests, an extensive experiment on the Spin Echo Small Angle Neutron Scattering spectrometer at the Reactor Institute Delft has been set up. This unique facility allows for the 'in bulk' determination of the particle (size) - particle (size) correlation function. More details on this work are described in an accompanying paper.

To enable the three-dimensional simulation of phase separation in bitumen, in the following the governing equations are derived.

3 Constitutive framework for bituminous healing simulation

3.1 Governing equations of phase separation

To develop the governing equations for the phase-separation model, the general mass conservation for phase α can be found as

$$\rho \frac{\partial \alpha c}{\partial t} = -\nabla \cdot (\alpha \rho (\alpha \underline{v} - \underline{v})) = -\nabla \cdot \alpha \underline{j} \quad (9)$$

In this, the term $\alpha \underline{v} - \underline{v}$ is the diffusion velocity and the term $\alpha \rho (\alpha \underline{v} - \underline{v})$ is the momentum of phase α , which can be represented by the mass diffusion flux $\alpha \underline{j}$.

This mass diffusion flux can also be expressed in terms of the gradient of the functional derivative of the free energy function Ψ

$$\begin{aligned} \alpha \underline{j} &= -\rho \alpha \underline{M} \cdot \nabla \left(\frac{\partial \Psi}{\delta \alpha c} \right) \\ &= -\rho \alpha \underline{M} \cdot \nabla (\alpha \mu) \end{aligned} \quad (10)$$

in which $\alpha \mu$ is the chemical potential of phase α and $\alpha \underline{M}$ is the diffusional mobility tensor of phase α in the material.

Replacing Eq. (10) into Eq. (9) gives the governing transport equation

$$\rho \frac{\partial \alpha c}{\partial t} - \text{div}(\rho \alpha \underline{M} \cdot \nabla \alpha \mu) = 0 \quad (11)$$

This formulation is also known as the Cahn Hilliard equation. In Cahn-Hilliard-based models, sharp interfaces are replaced by narrow transition layers (diffuse interfaces) that result from a competition between the different terms in the energy density

The chemical potential $\alpha \mu$ can be written as the functional derivative of the free energy

$$\alpha \mu = \frac{\delta \Psi}{\delta \alpha c} \quad (12)$$

The free energy is composed of three terms

$$\Psi = \Psi_0 + \Psi_\gamma + \Psi_\varepsilon \quad (13)$$

where Ψ_0 is the configurational free energy, Ψ_γ is the surface free energy and Ψ_ϵ is the strain energy.

Substituting Eq. (13) into Eq. (12) gives

$$\alpha\mu = \frac{\delta\Psi}{\delta_{\alpha}c} = \frac{\delta\Psi_0}{\delta_{\alpha}c} + \frac{\delta\Psi_\gamma}{\delta_{\alpha}c} + \frac{\delta\Psi_\epsilon}{\delta_{\alpha}c} \quad (14)$$

Using Eq (4), the configurational free energy Ψ_0 can be expressed as

$$\Psi_0(\alpha c, \beta c, T) = \sum_{\alpha=1}^n (\alpha c \alpha g + RT \alpha c \ln(\alpha c)) + RT \sum_{\alpha=1}^n \sum_{\beta>\alpha}^n \alpha c \beta c X^{\alpha\beta} \quad (15)$$

with the mixing energy expressed as

$$H(c) = \sum_{\alpha=1}^n \sum_{\beta>\alpha}^n \alpha c \beta c X^{\alpha\beta} \quad (16)$$

in which $X^{\alpha\beta}$ is the Flory Huggins interaction parameter between the phases and can be found from the solubility parameters of the phases α and β as:

$$X^{\alpha\beta} = \frac{\alpha V}{RT} (\beta \delta - \alpha \delta)^2 \quad (17)$$

in which αV is the molar volume of fraction αc and $\alpha \delta$ and $\beta \delta$ are the solubility parameters of the two fractions. The term $\alpha \delta^2$ is also known as the cohesive energy of fraction α .

For a biphasic material, Eq. (15) can be written as

$$\Psi_0(1c, T) = (1c \ 1g + (1-1c) \ 2g) + \left(RT \ 1c \ \ln(1c) + RT(1-1c) \ln(1-1c) + RT \ 1c \ (1-1c) X^{12} \right) \quad (18)$$

In which the second part of the free energy is often referred to as the chemical free energy or as the Flory Huggins free energy:

$$\Psi_{FH}(c,T) = RTc \ln(c) + RT(1-c) \ln(1-c) + RTc(1-c)X^{12} \quad (19)$$

The Flory Huggins interaction parameter X^{12} is controlling the shape of the chemical free energy. For $X^{12} \leq 2$ it has a single well and results in a single phase. In the case of $X^{12} > 2$ it is non-convex and has two wells, driving thus the phase separation into two binodal points (Fig. 13).

The surface free energy Ψ_γ was formulated by Cahn and Hilliard as

$$\Psi_\gamma = \kappa_1 \nabla^2 c + \kappa_2 \nabla_\alpha c \cdot \nabla_\alpha c \quad (20)$$

in which κ_1 and κ_2 are constants associated with gradients of compositions

The Ψ_ε is the Helmholtz free energy associated with the deformation of the material and is elaborately described in many publications [e.g. Holzaphel 2001, Scarpas 2005, Kringos et al. 2007].

Utilizing the above equations, integrating by parts, applying the divergence theorem and applying the Galerkin method, allows for a formulation which can be solved in the finite element method [Kringos 2011]:

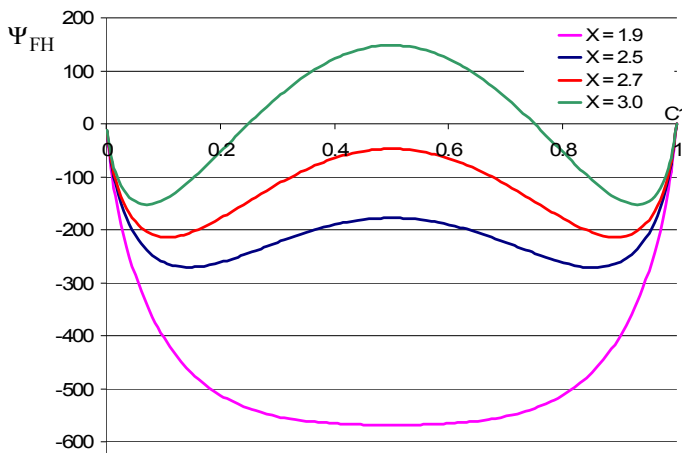


Figure 13: Convex and non-convex shape of Ψ_{FH} depending on X^{12}

$$\left[\begin{array}{l} N_i \left(\frac{\partial \rho}{\partial c} (c_n - c^t) + \rho_n \right) N_j \\ + \Delta t \nabla N_i \left\{ \frac{\partial \rho M}{\partial c} \left[\left(\frac{\partial^2 \Psi_0}{\partial c^2} + \kappa \right) c_k - \kappa \bar{c}_k \right] \nabla N_k + (\rho M) \frac{\partial^3 \Psi_0}{\partial c^3} \nabla N_k c_k \right\} N_j \\ + \Delta t \nabla N_i (\rho M) \left(\frac{\partial^2 \Psi_0}{\partial c^2} + \kappa \right) \nabla N_j \\ \left[-N_i N_j \right] \end{array} \right] \left\{ \begin{array}{l} [-\Delta t \nabla N_i (\rho M)_n \kappa \nabla N_j] \\ [N_i N_j + \nabla N_i \cdot \lambda^2 \nabla N_j] \end{array} \right\} \left\{ \begin{array}{l} \delta c_j \\ \delta \bar{c}_j \end{array} \right\} = - \left\{ \begin{array}{l} f_i^c \\ f_i^{\bar{c}} \end{array} \right\} \quad (21)$$

in which N_i are the shape functions and $\kappa = \frac{2 \kappa_2}{\lambda^2}$ is defined as the Cahn Hilliard parameter.

3.2 Simulation of phase rearrangements in the bituminous phase

The equations described in the previous section have been implemented for a bi-phasic mixture within the framework of the CAPA-3D software platform [Scarpas 2001]. Choosing the solubility parameters and temperature such that a natural phase separation in the bitumen will occur, the model is capable of simulating the formation of distinct clusters within the initially homogeneous bitumen, Figure 14, similar as was seen in the AFM scans.

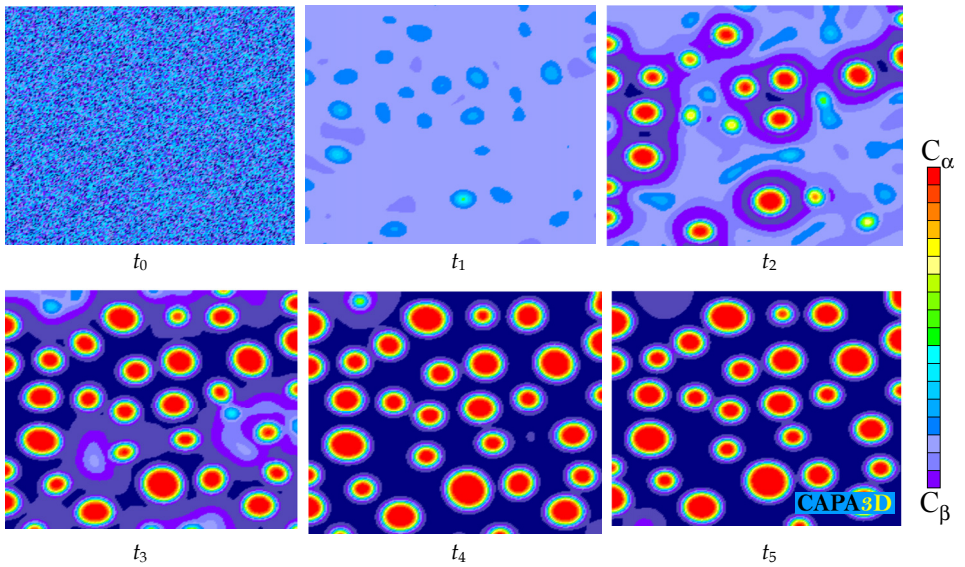


Figure 14: CAPA-3D simulation of phase separation in bitumen

The resulting inhomogeneous pattern can be easily brought back to its original, more homogeneous, structure by changing the temperature back to a convex situation, such as illustrated in Figure 12. In the model, there are several parameters which need to be calibrated such as, κ_1 and κ_2 which are associated with the kinetic efficiency for the material to create interfaces, Figure 15, and the parameter λ which is introduced into the model to avoid the use of higher order elements and which is controlling the thickness of the interfaces between the phases and is therefore an important parameter in the resulting crazing and healing cycle. Considering the nanometer scale of the interfaces, this is in fact a parameter which can only be found from an interactive procedure between the computational model and the available experimental characterization techniques.

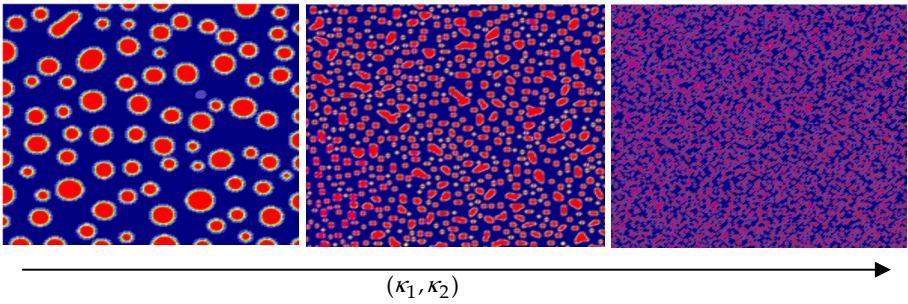


Figure 15: The dispersion of phases, controlled by κ_1 and κ_2

3.3 Integration of phase behaviour to elasto-visco-plastic constitutive model

Asphalt is known to be a material whose behaviour, depending on strain rate and temperature, exhibits response characteristics varying anywhere between the elasto-plastic and the visco-elastic limits. Constitutive models for such types of materials can be developed by combining the features of purely elasto-plastic and purely visco-elastic materials to create a more general category of constitutive models termed elasto-visco-plastic.

To define the general frame-work of the energy based constitutive model, the Helmholtz free energy function is expressed as

$$\Psi = \Psi_v(\mathbf{C}_e) + \Psi_p(\mathbf{C}_\infty, \xi_p) \quad (22)$$

in which $\psi_v(\mathbf{C}_e)$ is the viscous strain energy function, $\mathbf{C}_e = \mathbf{F}_e^T \mathbf{F}_e$ is the Cauchy-Green strain tensor, based on the deformation gradient \mathbf{F}_e , $\psi_p(\mathbf{C}_\infty, \xi)$ is the plastic free energy function, $\mathbf{C}_\infty = \mathbf{F}_\infty^T \mathbf{F}_\infty$ is the Cauchy-Green strain tensor based on the deformation gradient \mathbf{F}_∞ and ξ_p is the equivalent plastic strain.

From the second law of thermodynamics, the dissipation inequality can be found as

$$\mathbf{S} : \frac{1}{2} \dot{\mathbf{C}} - \left[\frac{\partial \Psi_v}{\partial \mathbf{C}_e} : \dot{\mathbf{C}}_e \right] - \left[\frac{\partial \Psi_p}{\partial \mathbf{C}_\infty} : \dot{\mathbf{C}}_\infty + \frac{\partial \Psi_p}{\partial \xi_p} : \dot{\xi}_p \right] \geq 0 \quad (23)$$

where \mathbf{S} is the second Piola-Kirchhoff stress tensor. It can be shown that from the above inequality the stress tensor \mathbf{S} can be additively decomposed into the visco-elastic \mathbf{S}_e and the elasto-plastic plastic component \mathbf{S}_∞

$$\begin{aligned} \mathbf{S} &= 2\mathbf{F}_v^{-1} \frac{\partial \Psi_v}{\partial \mathbf{C}_e} \mathbf{F}_v^{-T} + 2\mathbf{F}_p^{-1} \frac{\partial \Psi_p}{\partial \mathbf{C}_\infty} \mathbf{F}_p^{-T} \\ &= \mathbf{S}_e + \mathbf{S}_\infty \end{aligned} \quad (24)$$

Furthermore, the following inequalities are obtained

$$2\mathbf{F}_e \frac{\partial \Psi_v}{\partial \mathbf{C}_e} \mathbf{F}_e^T \mathbf{F}_e^{-T} : \mathbf{F}_e l_v \geq 0 \quad (25)$$

$$2\mathbf{F}_\infty \frac{\partial \Psi_p}{\partial \mathbf{C}_\infty} \mathbf{F}_\infty^T \mathbf{F}_\infty^{-T} : \mathbf{F}_\infty l_p - \frac{\partial \Psi_p}{\partial \xi_p} \dot{\xi}_p \geq 0 \quad (26)$$

To allow for the healing capacity of the material, as was discussed in the previous section, Eq. (26) can be modified with an additional term as:

$$2\mathbf{F}_\infty \frac{\partial \Psi_p}{\partial \mathbf{C}_\infty} \mathbf{F}_\infty^T \mathbf{F}_\infty^{-T} : \mathbf{F}_\infty l_p - \frac{\partial \Psi_p}{\partial \xi_p} \dot{\xi}_p + \frac{\partial \Psi_p}{\partial \xi_h} \dot{\xi}_h \geq 0 \quad (27)$$

In which the plastic free energy function Ψ_p has now, in addition to strain and plastic hardening, also an extra intrinsic parameter ξ_h which is named the ‘‘equivalent healing parameter’’:

$$\Psi_p = \Psi_p(\mathbf{C}_\infty, \xi_p, \xi_H(\phi_i)) \quad (28)$$

This equivalent healing parameter must be a function of all the healing related properties ϕ_i discussed in the previous sections, such as, among others, the number of clusters, the thickness of the interfaces, the rate of phase movement and the level of oxidation of the material. To demonstrate the capability of this model, the modified elasto-visco-plastic constitutive model is used in a simulation of a three-point-bending test, Figure 16.

In the simulation, the beam is first pushed down 40 mm and then pulled back up 20 mm. After this, the beam is pushed back into a “zero stress” situation. At this stage the beam is allowed to “rest” to allow for the micro-scale reorientation of the material that causes healing. After this rest period, the beam is pushed down again. In the case of the beam in which the healing model has not been activated, it takes a considerable lower force to push the beam back to its displacement from the previous loading cycles. This shows that the material has accumulated permanent damage and is weakened. In the case of the beam which did have the healing model active, the material seems to have lost its memory of the previous loading cycle, and the beam behaves as though no damage was induced.

4 Continuation of the research

In this paper the concept and general formulation of the multi-scale model for simulating of the mechanism of healing in bituminous materials has been discussed. The paper has given an overview of the theory behind the developed model and has shown some of the governing equations. In the continuation of this research the material parameters on nano- and micro-scale as discussed in this paper will be further determined. As more experimental data will become available, the healing functions as described in the beam-simulation will become better defined and, in the outset, should become available to be used in the production and design process of asphaltic pavements.

The main objective of the final model will be to enable a more accurate prediction of the healing capacity of bitumen, based on the physico-chemical parameters which can be determined in the lab. This will assist bitumen manufacturers as well as pavement

engineers to make a better choice for their bitumen blends to ensure better long-term performance of the asphaltic mixes.

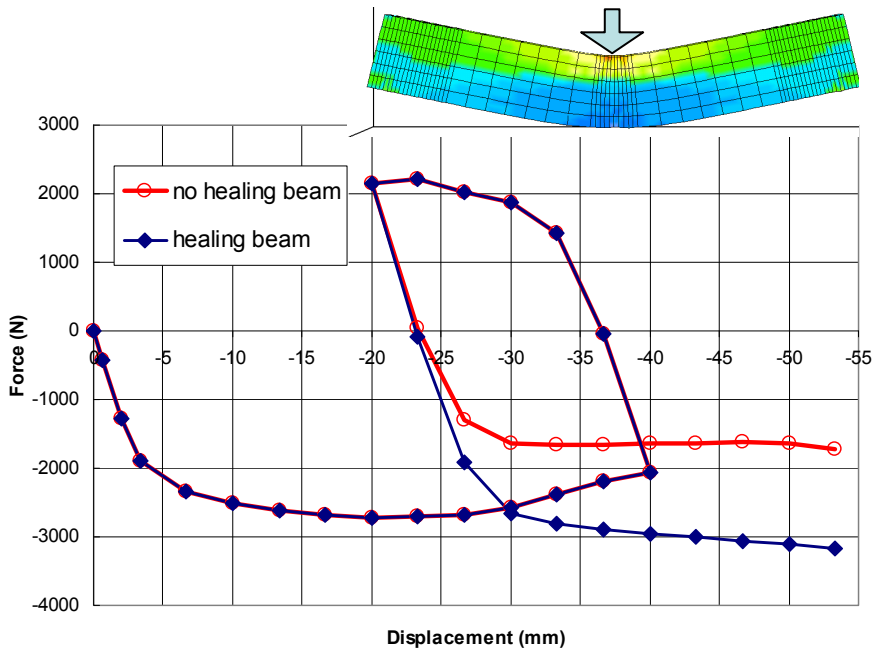


Figure 16: Simulation of healing versus non-healing asphalt beam

Acknowledgements

The research described in this paper has been performed in the context of the 'Delft Healing Consortium'. In this context, the authors gratefully acknowledge the support of Shell Global Solutions, Nynas AB, the Dutch Ministry of Public Works, Ooms Nederland Holding bv, the Delft Centre for Materials Research, the Western Research Institute and the US Federal Highway Administration. The first author would also like to thank the Dutch national science foundation STW, for the personal VENI grant, under which parts of this research was performed.

References

- [1] M.A. Bates, D. Frenkel. "Influence of polydispersity on the phase behavior of colloidal liquid crystals: A monte carlo simulation study". *The Journal of Chemical Physics*, 109(14):6193–6199, 1998
- A.T. Pauli, J.F. Branthaver, R.E. Robertson, W. Grimes, C.M. Eggleston, "Atomic Force Microscopy Investigation of SHRP Asphalts", *American Chemical Society, Division of Petroleum Chemistry*, 46(2), 104-110, 2001
- A. Scarpas, CAPA-3D Finite Element System User Manual, Delft University of Technology Publication 2001
- A. Scarpas, *A Mechanics based Computational Platform for Pavement Engineering*, Delft press, 2005
- [2] M. Bée, *Quasielastic neutron scattering: principles and applications in solid state chemistry, biology, and materials science*. Adam Hilger, Bristol and Philadelphia, 1988
- [3] J.F. Branthaver, J.C. Petersen, R.E. Robertson, J.J. Duvall, S.S. Kim, T. Harnsberger, P.M. adn Mill, E.K. Ensley, F.A. Barbour, and J.F. Schabron. *Binder characterisation and evaluation*, Vol. 2: chemistry. Technical Report SHRP-A-368, Strategic Highway Research Program, National Research Council, National Research Council, 2101 Constitution Avenue, NW Washington, DC 20418 USA, 1993
- [4] Z. Burton, B. Bhushan, Surface characterization and adhesion and friction properties of hydrophobic leaf surfaces. *Ultramicroscopy*, 106(8-9):709 – 719, 2006. Proceedings of the Seventh International Conference on Scanning Probe Microscopy, Sensors and Nanostructures, Proceedings of the Seventh International Conference on Scanning Probe Microscopy, Sensors and Nanostructures
- [5] L. Carboognani, L. , DeLima, M. Orea, U. Ehrmann, Studies of large crude oil alkanes. ii. isolation and characterization of aromatic waxes and waxy asphaltenes. *Petrol. Sci. Techn.*, 18:607–34, 2000
- J.W. Cahn, J.E. Hilliard, "Free energy of a nonuniform system. I. Interfacial energy," *J. Chem. Phys.* 28, 258, 1958
- [6] P. Claudy, J.M. Letoffe, G.N. King, J.P. Planche. Characterization of asphalts cements by thermomicroscopy and differential scanning calorimetry : correlation to classic physical properties. *Fuel science & technology international*, 10(4-6):735–765, 1992
- [7] D.L. Dorset. *Crystallography of the Polymethylene Chain: An Inquiry into the Structure of Waxes*, volume 17 of International Union of Crystallography Monographs on Crystallography. Oxford University Press, 2005

- [8] H.J. Ensikat, M. Boese, W. Mader, W. Barthlott, K. Koch. Crystallinity of plant epicuticular waxes: electron and x-ray diffraction studies. *Chemistry and Physics of Lipids*, 144(1):45 – 59, 2006
- [9] I. Gawel, F. Czechowski, and K. Baginska. Study of wax isolated from bitumen. In Proceedings of Eurasphalt & Eurobitume Congress, page 139, May 7-10 1996
- [10] J.P. Hansen and I.R. McDonald. *Theory of simple liquids*. Academic Press, 2006
- G. Holzaphel, *Nonlinear Solid Mechanics: A Continuum Approach for Engineering*, John Wiley & Sons, 2001
- [11] D.R. Jones. Shrp materials reference library, asphalt cements: A concise data compilation. Technical Report SHRP-A-645, Strategic Highway Research Program, National Research Council, Washington DC, USA, National Research Council, 2101 Constitution Avenue, NW Washington, DC 20418 USA, 1993
- D.R. Jones, T.W. Kennedy, 'Asphalt Chemistry and its Effects on Roadway Surface Conditions'
- [12] M. Kané, M. Djabourov, J.-L. Volle, J.-P. Lechaire, and G. Frebourg, Morphology of paraffin crystals in waxy crude oils cooled in quiescent conditions and under flow. *Fuel*, 82(2):127–135, 2003
- [13] N. Kringos, A. Scarpas, T. Pauli, and R. Robertson. A thermodynamic approach to healing in bitumen. In Andreas Loizos, Manfred N. Partl, and Tom Scarpas, editors, *Advanced Testing and Characterization of Bituminous Materials*, pages 123–128. Taylor & Francis, 2009
- N. Kringos, A. Scarpas, C. Kasbergen, Three Dimensional Elasto-Visco-Plastic Finite Element model for Combined Physical-Mechanical Moisture Induced Damage in *Asphaltic Materials*, Journal of the Association of Asphalt Paving Technologists, Vol.76, 2007
- [14] R. E. Lechner, R. Melzer, and J. Fitter. First qins results from the tof-spectrometer neat. *Physica B: Condensed Matter*, 226(1-3):86 – 91, 1996
- [15] L. Loeber, O. Sutton, J. Morel, J.-M. Valleton, and G. Muller. New direct observations of asphalts and asphalt binders by scanning electron microscopy and atomic force microscopy. *Journal of Microscopy*, 182(1):32–39, 1996
- [16] S.W. Lovesey. *Theory of neutron scattering from condensed matter*. Oxford University Press, USA, 1986
- [17] Xiaohu Lu, M. Langton, P. Olofsson, and P. Redelius. Wax morphology in bitumen. *Journal of Materials Science*, 40(8):1893–1900, April 2005

- [18] Xiaohu Lu, P. Redelius. Effect of bitumen wax on asphalt mixture performance. *Construction and Building Materials*, 21(11):1961–1970, 2007
- D.N. Little, A. Bashin, ‘Exploring Mechanisms of Healing in Asphalt Mixtures and Quantifying Its Impact’, in *Self Healing Mateterials: an alternative approach to 20 centuries of materials science*, Springer Series in Materials Science 100, 2007
- [19] J.F. McKay, J.F. Branthaver, and Robertson R.E. Isolation of waxes from asphalts and the influence of waxes on asphalt rheological properties. Preprints - American Chemical Society. Division of Petroleum Chemistry, ACS 210th National Meeting, Chicago, IL, August 20–25, 1995
- [20] B. J. Musser, P.K. Kilpatrick. Molecular characterization of wax isolated from a variety of crude oils. *Energy & Fuels*, 12(4):715–725, July 1998
- [21] J.C. Petersen, R.E. Robertson, J.F. Branthaver, P.M. Harnsberger, J.J. Duvall, S.S. Kim, D.A. Anderson, D.W. Christiansen, H.U. Bahia, R. Dongre, C.E. Antle, M.G. Sharma, J.W. Button, and C.J. Glover. Binder characterization and evaluation, vol. 4: Test methods. Technical Report SHRP-A-370, Strategic Highway Research Program, National Research Council, Washington DC, USA, National Research Council, 2101 Constitution Avenue, NW Washington, DC 20418 USA, 1994
- [22] P. Redelius. *Hansen Solubility Parameters; A user’s handbook*, chapter Hansen solubility parameters of asphalt, bitumen and crude oils, pages 151–158. CRC Press, 2nd edition, 2007
- [23] P. Redelius, X. Lu, and U Isacson. Non-classical wax in bitumen. *Road Materials and Pavement Design*, 3(1):7–21, 2002
- [24] M.T. Rekveldt, J. Plomp, W.G. Bouwman, W.H. Kraan, S. Grigoriev, M. Blaauw. Spin-echo small angle neutron scattering in Delft. *Review of Scientific Instruments*, 76(3):033901, 2005
- [25] R. E. Robertson, K. P. Thomas, P. M. Harnsberger, F. P. Miknis, T. F. Turner, J. F. Branthaver, S-C. Huang, A.T. Pauli, D. A. Netzel, T. M. Bomstad, D. Farrar, M.J. Sanchez, J. F. McKay, and M. McCann. Fundamental properties of asphalts and modified asphalts ii, final report, volume i: Interpretive report. Technical report, Federal Highway Administration, Contract No. DTFH61-99C-00022, March 2006
- [26] S.P. Srivastava, Jyoti Handoo, K.M. Agrawal, and G.C. Joshi. Phase-transition studies in n-alkanes and petroleum-related waxes—a review. *Journal of Physics and Chemistry of Solids*, 54(6):639–670, 1993
- [27] S. N. Taraskin, Y. L. Loh, G. Natarajan, and S. R. Elliott. Origin of the boson peak in systems with lattice disorder. *Phys. Rev. Lett.*, 86(7):1255–1258, Feb 2001

- [28] T.F. Turner and J.F. Branthaver. *Asphalt Science and Technology*, chapter DSC studies of asphalts and asphalt components, pages 59–101. Marcel Dekker, Inc., New York, 1997
- [29] F.M. van der Kooij, K. Kassapidou, H.N. W. Lekkerkerker. Liquid crystal phase transitions in suspensions of polydisperse plate-like particles. *Nature*, 406(6798):868–871, August 2000
- [30] M. Zbik, R.G. Horn, N. Shaw. Afm study of paraffin wax surfaces. *Colloids and Surfaces A: Physicochemical and Engineering Aspects*, 287(1-3):139 – 146, 2006
- [31] N. Kringos, A. Schmets, T. Pauli and A. Scarpas, *A Finite Element Based Chemo-Mechanics Model to Simulate Healing of Bituminous Materials*, *Chemo-Mechanics of Bituminous Materials*, ISBN/EAN 978-94-90284-04-9, p.69-75
- [32] N. Kringos et al., Parametric Analyses of Three Dimensional Phase Separation of Bitumen, in preparation
N. Kringos, Exploring the Kinetics of Phase Decomposition to Understand Behavior of Bitumen, under review, 2011
- [33] S.A.M. Hesp, S. Iliuta, J.W. Shirokoff, Reversible aging in asphalt binders, *Energy and Fuels*, 21 (2), 1112-1121, 2007
- [34] F. Hammoumm, C. de La Roche, J.M. Piau, C. Stefani, Experimental investigation of fracture and healing of bitumen at pseudo-contact of two aggregates, Ninth ISAP International Conference on Asphalt Pavements, Denmark, 2002
- [35] X. Lu, H. Soenen, P. Redelius, Fatigue and healing characteristics of bitumens studied using dynamic shear rheometer, 6th RILEM Conference PTEBM'03, Zurich, 2003
- [36] M.C. Philips, Multi-step models for fatigue and healing and healing and binder properties involved in healing, Eurobitume Workshop 99, Luxembourg, 1999
- [37] Y.R. Kim, D.N. Little, F.C. Benson, Chemical and mechanical evaluation on healing mechanism of asphalt concrete, Proceedings Association Asphalt Paving Technologists, Vol. 59, 1990